

This is an Open Access document downloaded from ORCA, Cardiff University's institutional repository:<https://orca.cardiff.ac.uk/id/eprint/145264/>

This is the author's version of a work that was submitted to / accepted for publication.

Citation for final published version:

Ma, Shuai, Tang, Qian, Liu, Ying and Feng, Qixiang 2022. Prediction of mechanical properties of 3d printed lattice structures through machine learning. *Journal of Computing and Information Science in Engineering* 22 (3) , 031008. 10.1115/1.4053077

Publishers page: <https://doi.org/10.1115/1.4053077>

Please note:

Changes made as a result of publishing processes such as copy-editing, formatting and page numbers may not be reflected in this version. For the definitive version of this publication, please refer to the published source. You are advised to consult the publisher's version if you wish to cite this paper.

This version is being made available in accordance with publisher policies. See <http://orca.cf.ac.uk/policies.html> for usage policies. Copyright and moral rights for publications made available in ORCA are retained by the copyright holders.



Prediction of Mechanical Properties of 3d Printed Lattice Structures through Machine Learning

Shuai Ma

State Key Laboratory of Mechanical Transmissions, Chongqing University
Chongqing, 400044, China
ms@cqu.edu.cn
Student Mem. ASME

Qian Tang¹

State Key Laboratory of Mechanical Transmissions, Chongqing University
Chongqing, 400044, China
tqcqu@cqu.edu.cn

Ying Liu

Institute of Mechanical and Manufacturing Engineering, School of Engineering, Cardiff University
Cardiff, CF24 3AA, UK
LiuY81@cardiff.ac.uk
Mem.ASME

Qixiang Feng

State Key Laboratory of Mechanical Transmissions, Chongqing University
Chongqing, 400044, China
fengq2@cqu.edu.cn

ABSTRACT

Lattice structures (LS) manufactured by 3D printing are widely applied in many areas, such as aerospace and tissue engineering, due to their lightweight and adjustable mechanical properties. It is necessary to reduce costs by predicting the mechanical properties of LS at the design stage since 3D printing is exorbitant at present. However, predicting mechanical properties quickly and accurately poses a challenge. To address this problem, this study proposes a novel method that is applied to different LS and materials to predict their

¹ Corresponding author.

36 *mechanical properties through machine learning. First, this study voxelised 3D models of the LS units and*
37 *then calculated the entropy vector of each model as the geometric feature of the LS units. Next, the porosity,*
38 *material density, elastic modulus, and unit length of the lattice unit are combined with entropy as the inputs*
39 *of the machine learning model. The sample set includes 57 samples collected from previous studies. Support*
40 *vector regression was used in this study to predict the mechanical properties. The results indicate that the*
41 *proposed method can predict the mechanical properties of LS effectively and is suitable for different LS and*
42 *materials. The significance of this work is that it provides a method with great potential to promote the*
43 *design process of lattice structures by predicting their mechanical properties quickly and effectively.*

44 **Keywords:** *Lattice structures; mechanical properties; 3D printing; machine learning*

45

46 **1. INTRODUCTION**

47

48 Lattice structures (LS), whether inspired by nature or created by mathematicians,
49 are considered promising candidates for lightweight energy absorption and heat
50 dissipation because their unique geometric shape can realise different functions. As
51 FIGURE 1 shows, the most applied LS are body-centred cubic (BCC) [1], face-centred cubic
52 (FCC) [2], BBC with vertical struts (BCCZ) [3], and triply periodic minimal surface (TPMS)
53 structures [4]. Parts composed of LS are designed by arraying the LS unit; however, they
54 are hard to fabricate via traditional manufacturing methods because of their complex
55 interior shapes.

56 Additive manufacturing (AM), also called 3D printing, is an advanced
57 manufacturing technology to fabricate complex parts that cannot be manufactured by
58 traditional technology. AM includes various manufacturing methods, such as fused
59 deposition modelling, electron beam melting, selective laser melting (SLM), and selective
60 laser sintering. These methods also allow the manufacture of parts using non-metallic and

61 metallic materials. SLM is widely applied in aerospace, automotive, and tissue engineering
62 and moulds because it allows the use of many metallic powders: Ti6Al4V [5], stainless
63 steel 316L [6], and maraging steel [7]. Furthermore, the layer-by-layer fabricated feature
64 of SLM can freely manufacture samples with complex shapes and internal structures.
65 Thus, SLM is considered a promising manufacturing method for fabricating metallic parts
66 composed of LS.

67 The mechanical properties of LS are the basic requirements when they are used in
68 various applications. LS have many advantages, and their elastic modulus and yield
69 strength can be adjusted by designing with different unit parameters. This can save
70 materials by choosing a suitable lattice structure to match the mechanical requirements.
71 The elastic modulus is one of the most important mechanical properties of LS; it can
72 achieve around 1% to 100% of the elastic modulus of solid material by manufacturing with
73 different designed parameters.

74 In some application areas, the mechanical properties of parts composed of LS have
75 strict design requirements. These include SLM-built bone scaffolds; as shown in FIGURE
76 2, the mechanical properties of the implanted scaffold should match those of damaged
77 human bones to avoid “stress-shielding”, which may lead to bone osteoporosis [8].
78 Furthermore, these kinds of porous scaffolds can also satisfy other functional
79 requirements, such as good mass-transporting requirements [9].

80 Yield strength is another important mechanical property of parts composed of LS;
81 parts will undergo permanent deformation if the loading stress is higher than yield
82 strength. Thus, studying the yield strength of the LS can guide us to avoid parts failure.

83 Estimating the elastic modulus and yield strength of LS quickly can help designers
84 choose a suitable structure accurately and shorten the design time of parts. In general,
85 the elastic modulus and yield strength are calculated using the strain-stress diagram
86 obtained from compressive experimentation on LS samples. However, fabricating all LS
87 samples with different designed parameters to study their mechanical properties and
88 thereby choose the most suitable structure is expensive and time-consuming, especially
89 since multiple candidate structures and materials are involved.

90 Finite element analysis (FEA) seems to be a promising method to predict the
91 mechanical properties of LS because it only requires the 3D model of the LS. However,
92 this method has certain disadvantages that limit its use. First, most 3D models of the LS
93 are outputted as .stl files by modelling or programming software. These .stl files cannot
94 be meshed directly by the simulation software; they need to be solidified first, and this
95 process may cause the 3D models to lose some details of geometric features. In addition,
96 the parameters of simulation need to be set for each 3D model, and the simulation usually
97 takes hours. Therefore, finding a quick and accurate method to predict the mechanical
98 properties of LS remains a challenge.

99 With the development of computer power, data collection, and algorithms,
100 machine learning has been used in many areas because it can build a predictive model
101 based on a wide variety of input features and predict the target result. Naif et al. used
102 convolutional neural networks to predict porous media properties from 2D micro-
103 computed tomography images [10]. Jinlong built a model to predict the permeability of
104 porous samples from images; the results showed that, compared with FEA, this machine

105 learning method can reduce the computational time by several orders of magnitude [11].
106 Therefore, machine learning offers the possibility to predict the mechanical properties of
107 LS quickly. This paper proposes a novel method that can predict the mechanical
108 properties of various LS and materials by machine learning. The entropy of the 3D model
109 of LS, which represents the geometric characteristics of different LS units, together with
110 general design parameters for different LS (such as the porosity, unit length, and elastic
111 modulus of solid materials), are adopted as input features for the machine learning.
112 Support vector regression (SVR) is then used to fit and predict the elastic modulus and
113 yield strength of 57 LS models. These input features are easy to obtain, and once the
114 predictive model is built, the prediction process is completed in a matter of seconds.

115 This paper bases on previous work [12] and presents a novel method to predict
116 the mechanical properties of 3D printed samples composed of different LS and materials.
117 The related literature is presented in section 2, and the input features and prediction
118 method are introduced in section 3. The evaluation of the predictive model and the
119 comparison of measured and predicted values of elastic modulus and yield strength of LS
120 samples are discussed in section 4. Conclusions and prospects for future studies are
121 outlined in section 5.

122

123 **2. LITERATURE REVIEW**

124 **2.1 Prediction method of mechanical properties of LS**

125

126 Elastic modulus and yield strength were calculated from the strain-stress diagram, based
127 on the compressive experiments. The compressive experiment is the most basic and
128 accurate method for investigating the mechanical properties of LS. Sing et al. studied the

129 mechanical properties of Ti6Al4V LS in different orientations and densities [13]. FEA is a
130 common method for predicting the mechanical properties of complex models. Maskery
131 et al. compared the mechanical properties of gyroid, diamond, and primitive LS through
132 both experimental and simulated methods: their results showed that the error of elastic
133 modulus ranged from 4% to 18% [14]. However, the prediction accuracy of FEA fluctuated
134 because the LS were too complex and there were some manufacturing defects in the as-
135 built samples. Arun et al. studied the mechanical properties of six porous scaffolds by
136 experimental and simulated methods: the best-predicted errors for elastic modulus and
137 yield strength were 19.6% and 24.7%, respectively [15]. Shuai et al. built and studied (by
138 FEA) the mechanical properties of five gyroid structures with 75.1% to 88.8% porosities;
139 prediction accuracy ranged from 30% to 56% [9]. Kevin et al. investigated the mechanical
140 properties of seven strut structures through compressive experiments and predicted
141 them using simulated and analytical methods; the highest predicted error could reach
142 300% to 400% [16].

143 The experimental and simulated method is not only expensive but also time-consuming.
144 Other researchers have proposed fitting formulae: Maxwell et al. built a multiple linear
145 regression model to predict the mechanical properties of stochastic lattice structures in
146 terms of density, fabric, and eigenvalue. For elastic modulus, the off-axis properties
147 ranged from 4.2% to 13%, and the coefficient of determination R^2 ranged from 0.84 to
148 0.97; for yield strength, the relative error ranged from 5.1% to 10%, and R^2 ranged from
149 0.84 to 0.94 [17]. Matteo et al. used the Gibson-Ashby equation to study the relationship
150 between the mechanical properties of LS and solid materials [18]: the R^2 values were all

151 greater than 0.98. Although it is quick to calculate elastic modulus by fitting functions in
152 this way, the function is only suitable for one structure and has limitations for predicting
153 various structures. Furthermore, Han et al. investigated the mechanical properties of
154 strut-based structures by structural mechanics analysis [19], but this only proved suitable
155 for simple strut structures and not for complex LS such as TPMS.

156 **2.2 Machine learning application in mechanical properties prediction**

157

158 With its development and successful application in different areas, machine learning has
159 attracted the attention of many researchers. Hany et al. used the shallow neural network,
160 deep neural network, and deep learning neural network to predict the mechanical
161 properties of the diamond lattice structure; the best mean percentage errors of elastic
162 modulus and yield strength were 14.6% and 5.26%, respectively [20]. However, the
163 authors only use strut length, diameter, and orientation angle as study features; these
164 features are not suitable for other kinds of structures. Mark et al. developed an adaptive
165 neural network-based model to predict femoral neck strains and fracture loads. Their
166 results were better than the finite element model, with the R^2 ranging from 0.84 to 0.98
167 [21]. Meng et al. predicted lumbar vertebral strength through a general regression neural
168 network and SVR according to the grayscale distribution of quantitative computed
169 tomography images, structural rigidity, and other features [22]. Zhenghua et al. used the
170 chemical composition and porosity of compacts as descriptors to predict the mechanical
171 properties of Cu-Al alloys. Six algorithms were introduced, of which SVR showed the best
172 prediction ability [23]. Together, these studies show the great application potential for

173 machine learning. In the context of this study, SVR was chosen to predict the mechanical
174 properties of LS.

175 **2.3 Geometric feature selection**

176
177 Bael et al. investigated the influence of geometry on the mechanical properties of LS.
178 Their results showed that the shapes of LS will significantly affect the mechanical
179 properties of parts. Parts composed of LS were arrayed by the LS units; thus, the
180 mechanical properties and geometric features of LS can be represented by the single unit
181 model, and the geometric features of unit 3D models were considered as the studied
182 features in this research.

183 In general, geometric features such as point cloud [24,25], feature curves [26,27], and
184 voxelisation [28] have been applied in parts retrieval and classification. Wei et al.
185 voxelised and calculated the entropy of 3D models to represent and retrieve different
186 machine parts [29], they all be proved as the promising methods to represent the
187 geometric features of 3d models. However, the point cloud method will generate tens of
188 thousands of coordinate data for each 3d model, and the complex internal shapes of LS
189 cannot be perfectly represented by the feature curves method. Thus, entropy vectors of
190 LS unit 3D models are applied as the input parameters of the prediction model.
191 Furthermore, Maskery et al. studied a series of 78% porosity gyroid parts with different
192 unit lengths (from 3 mm to 9 mm) and indicated that unit length would affect the
193 mechanical properties of parts [30]. Bartolomeu et al. studied the elastic modulus of
194 lattice structures with different porosities ranging from 64.2% to 93.3%; their elastic
195 modulus ranged from 28.6 GPa to 12.4 GPa [31]. In summary, entropy, porosity, unit

196 length, the density of LS unit, and elastic modulus of solid materials were considered as
197 features in this study.

198 **3. METHODOLOGY**

199 **3.1 Entropy of 3D models**

200
201 Typically, point cloud, view-based features, and feature curves are used in parts retrieval
202 to represent the geometric features of parts, and they all be proved as promising and
203 effective methods. However, for 3D printed structures, applying these methods results in
204 certain problems, such as too much data, errors caused by inconsistent viewing
205 directions, the difficulty of representing the complex internal structure of LS, and the
206 feature curves method cannot effectively represent the structures with the same
207 primitive surface. Thus, considering the universality of the method to the 3d models of
208 LS, the geometric features of different LS units could be represented by the entropy of
209 their voxelised 3D models.

210 Voxelisation involves converting the 3D model to a model consisting of pixels of a
211 specified size; the new model is located at a space with R^3 resolution. There are two kinds
212 of pixels in this space: empty and solid pixels. To calculate the entropy of a voxelised part,
213 first, the 3D models of LS units were voxelised into 3D voxels. To avoid too much data and
214 ensure sufficient precision, 20^3 , 50^3 , 100^3 , 150^3 , 200^3 , and 300^3 resolutions were tested.
215 The porosities of re-built voxelised models were calculated and compared with the 3d
216 models, thus, $100 \times 100 \times 100$ resolution was adopted in this study. As FIGURE 3 shows,
217 for the circle voxelised at $20 \times 20 \times 20$ resolution, the proportions of solid and empty

218 voxels were defined as P_1 , P_2 , respectively. Then, the entropy was calculated by the
219 equation [29]:

$$220 \quad H_2 = -P_1 \log_2 P_1 - P_2 \log_2 P_2 \quad (1)$$

$$221 \quad P_1 + P_2 = 1 \quad (2)$$

222 where H_2 represents the entropy of the 3D model.

223 The global entropy of the 3D model makes it difficult to distinguish different models with
224 the same P_1 and P_2 but which have different shapes. Thus, the voxelised models were
225 divided into 100 layers. To maintain consistency, the fabricated direction z-axis was
226 applied as the divided direction since the compression experiments were processed in
227 the same direction. As FIGURE 4 shows, 20 subspaces with $100 \times 100 \times 5$ resolution were
228 divided from each voxelised model, meaning that every five layers were divided into a
229 subspace. The H_2 value of each subspace was then calculated, and an entropy vector
230 composed of 20 entropy was obtained to represent the 3D model of the LS unit. The
231 entropy vectors of all samples were obtained using this method and applied as the 1 to
232 20 input features of the predictive model.

233 **3.2 Design parameters of lattice structures**

234

235 Modelling the 3D models of LS units is the first step in designing parts composed of porous
236 structures. Once the type of lattice structure is chosen, some parameters can still be
237 modified to obtain different unit cells. For strut-based structures, as shown in FIGURE 5
238 (a), the length and diameter of struts were used as the featured parameters. For surface-
239 based structures (one kind of TPMS), as shown in FIGURE 5 (b), the pore size and thickness
240 of the surface were applied.

241 However, to predict the mechanical properties of different structures using one predictive
242 model, common parameters that suit all kinds of LS must be considered in this study. As
243 FIGURE 5 (c) shows, L is the length of the unit; another common parameter is porosity (P),
244 as defined by the equation below:

$$245 \quad P = \left(1 - \frac{V_{solid}}{V_{cube}}\right) \times 100\% \quad (3)$$

246 where V_{solid} and V_{cube} are the volumes of the unit and the cube, respectively.

247 These two common parameters are suitable for all LS. Furthermore, for the prediction of
248 mechanical properties of LS manufactured with different materials, the density and
249 elastic modulus of solid metallic materials were also introduced as input features in the
250 machine learning model.

251 In summary, a total of 24 parameters were used as input features: 20 entropy of
252 subspaces, plus unit length, unit porosity, and density and elastic modulus of materials.

253 **3.3 Collection of study samples**

254
255 Considering that the information of structures given in the related papers is not complete
256 as input features. To obtain the complete data and correct 3d models, the details of fifty-
257 seven SLM samples (fabricated using Ti6Al4V and 316L stainless steel powders) were
258 collected from previous studies of the 3D printing research group, Chongqing University.
259 The 3D models of all LS units were re-built and outputted as .stl files using Rhino software.
260 Magics software was then used to convert all 3D models to the same accuracy of the
261 triangular patch (0.05 mm) in order to eliminate the influence of modelling accuracy. To
262 allow the predictive model to examine as many kinds of structures as possible, 11 kinds
263 of common LS units (with different designed parameters and materials) were introduced

264 in this study. These LS units are shown in TABLE 1. The study set included strut structures
 265 and strut-based and sheet-based TPMS structures.

266 To build the predictive model, 10 samples were randomly picked from the 57 study
 267 samples to compose the test set. The remaining samples were used as the training set.

268 **3.4 Algorithm and evaluation of prediction**

269
 270 SVR was used as the machine learning algorithm in this study. The grid search method
 271 and 10-fold cross-validation were conducted to obtain a robust predictive model. The
 272 predictive model was fitted using Pycharm software and the scikit-learn toolkit. The
 273 program was processed on Surface Pro 6 (Microsoft Corporation, i5-8350U, 8G RAM).

274 As FIGURE 6 shows, the 3D models of LS units were voxelised and divided into 20
 275 subspaces; the entropy of each subspace was calculated to obtain the entropy vector,
 276 which was then combined with other studied features as input parameters to train the
 277 predictive model (processed by SVR). The root mean squared error (RMSE) and
 278 determination (R^2) were introduced to evaluate the predictive model as the following
 279 equations:

$$280 \quad RMSE = \sqrt{\frac{1}{m} \sum_{i=1}^m (y_i - \hat{y}_i)^2} \quad (4)$$

$$281 \quad R^2 = 1 - \frac{\sum_{i=1}^m (\hat{y}_i - y_i)^2}{\sum_{i=1}^m (\bar{y} - y_i)^2} \quad (5)$$

282 where m is the number of samples, y_i , \hat{y}_i , and \bar{y} represent the actual, predicted and the
 283 average value of output. Furthermore, the predicted error (e) and relative error (e_r)
 284 between predictive and experimental mechanical properties are defined using the
 285 following equations:

286
$$e = |E_{pre} - E_{exp}| \quad (6)$$

287
$$e_r = \frac{|E_{pre} - E_{exp}|}{E_{exp}} \times 100\% \quad (7)$$

288 where E_{pre} and E_{exp} represent the predicted and experimental mechanical properties
289 (elastic modulus and yield strength) of LS, respectively.

290 Also, considering the time cost of the fitting formulae and structural mechanics analysis
291 is hard to measure, and FEA is the most common method to predict the mechanical
292 properties of LS, this study compared the current and FEA methods to evaluate the speed
293 and accuracy of this method.

294 **4. RESULTS AND DISCUSSION**

295

296 To assess whether entropy vectors can effectively represent the geometric features of
297 different structures, TABLE 2 shows the entropy distribution of four kinds of LS with
298 different design parameters. For the entropy distributions of different LS categories, the
299 shapes of the distribution are significantly different. However, the 3D models in the same
300 row belong to one kind of structure but with different design parameters, such as
301 diameter and porosity; their entropy distributions have the same shape but different
302 values. The results indicate that the entropy vectors are suitable for representing various
303 lattice structures; therefore, they provide a good group of input features for the machine
304 learning model.

305 The parameters of the predictive model were optimised using the grid search method.

306 The evaluation of the resulting model is shown in TABLE 3. For elastic modulus, in the
307 training set, the RMSE and R^2 reached 636 and 0.93, respectively. The results also indicate

308 that the geometric features of LS 3D models have a high correlation with elastic modulus.

309 Considering that the actual elastic modulus of the training set ranged from 68 MPa to
310 9,309 MPa, with 244 MPa predicted error and 5.6% relative error, the results are good for
311 this model. In the test set, the RMSE (885) is higher than in the training set. R^2 is 0.81,
312 which is slightly lower than in the training set, and the relative error reaches 24.6%.
313 Compared to the existing prediction methods outlined in section 2.1, their R^2 values
314 ranged from 0.84 to 0.98 and relative error from 4% to 18%. The results of this study show
315 that the current prediction method has great application potential.

316 In terms of the yield strength predictive model, the actual yield strength of all samples
317 ranged from 1.9 MPa to 590.3 MPa. In the training set, the RMSE and mean error were
318 25.96 MPa and 14.14 MPa, respectively, and the R^2 value reached 0.96, which
319 demonstrates a stronger correlation than the elastic modulus; however, the mean
320 relative error was 20.1%. The RMSE and R^2 of the test set were worse than in the training
321 set. Furthermore, the mean relative error is the highest at 40.9%; the reasons will be
322 analysed below.

323 FIGURE 7 (a) shows the actual and predicted elastic modulus of the training set. Most of
324 the predicted values have a strong correlation with the actual results. The largest
325 predicted error occurs in sample 22, a sheet-based I-WP structure with 55% porosity; the
326 error is 3,007 MPa. This may be because I-WP structures have greater mechanical
327 properties compared with other structures, and this error could be reduced by
328 introducing more samples with different parameters.

329 FIGURE 7 (b) shows the relative errors for the training set. The largest relative error
330 (47.9%) is observed in sample 8, an 85% porosity strut-based diamond structure whose

331 actual elastic modulus is only 1,074 MPa. Its predicted error is 514 MPa, which is slightly
332 higher than the mean error of the training set (244 MPa) and far below the maximum
333 error observed in sample 22.

334 To compare the actual and predicted results, 10 samples in the test set were inputted into
335 the predictive model; the results are shown in FIGURE 8. The largest errors were observed
336 in samples 2 and 7, which have roughly 55% porosity and belong to strut-based and sheet-
337 based Schwarz primitive structures, respectively. The possible reason for the error is that
338 the elastic modulus of LS will increase significantly as porosity decreases, and the
339 porosities of 44 of 57 samples were higher than 60%. With more lower-porosity samples,
340 the predicted results should show great improvement. For relative error, only sample 10
341 has 37.5 MPa actual elastic modulus, which will make the relative error sensitive to the
342 predicted difference.

343 FIGURE 9 shows the differences between actual and predicted yield strengths. Generally,
344 the predicted curve matched the actual curve well. The minimum predicted error is 0.97
345 MPa, while the maximum predicted error is 118.23 MPa. For sample 10, the strut-based
346 diamond structure, the actual value is 249.5 MPa. Except for three samples with high
347 predicted errors, the predicted errors of the other 44 samples were lower than 23.5 MPa.
348 Four relative errors are high, while the relative errors of the 43 remaining samples are
349 lower than 27%. The highest value is 164%: the relative error of sample 11, a strut-based
350 gyroid structure, which has 95% porosity and 6.1 MPa yield strength. However, the
351 predicted error of sample 11 is only 10 MPa, lower than the mean error of 14 MPa. The
352 mean relative error would reach 16.9% by excluding sample 11.

353 The maximum predicted error of the test set is 128.77 MPa, and the actual value of this
354 sample is 326 MPa. The errors for 8 out of 10 samples are lower than 40 MPa. As FIGURE
355 10 (b) shows, the relative error of sample 10 is 171%, but the predicted error is only 3.2
356 MPa, which has a significant effect on the mean relative error; if sample 10 is excluded, it
357 would decline to 26.4%.

358 Considering that even the mechanical properties obtained from the compression
359 experiments have fluctuating errors, as TABLE 4 shows, errors ranged from 33 MPa to 162
360 MPa, while the elastic modulus ranged from 1,465 MPa to 2,676 MPa [32]. Experimental
361 error ranged from 100 MPa to 130 MPa, and experimental elastic moduli of LS ranged
362 from 2,700 MPa to 3,600 MPa [33]. Furthermore, errors from 120 MPa to 3,640 MPa for
363 elastic modulus and 0.38 MPa to 12 MPa for yield strength have also been reported [16].
364 Thus, the predicted errors of 244 MPa to 593 MPa for elastic modulus and 14.14 MPa to
365 37.14 MPa for yield strength in this study still show good agreement, since the elastic
366 modulus and yield strength ranged from 37.5 MPa to 9,309 MPa and 1.9 MPa to 590.3
367 MPa, respectively.

368 As TABLE 5 shows, the results and time costs of the formula, FEA, and the current methods
369 are compared with ref [5]. The yield strength of all samples, and the elastic modulus of
370 complex structure Fcc-BCC, can not be predicted by the formula method. FEA method
371 exhibits the lowest error of predicted yield strength of BCC structures, while for complex
372 fcc-BCC structure, the SVR method shows higher accuracy. For the time consumption,
373 once the SVR model is built, the prediction will finish in about 5 secs, while FEA will cost
374 about 30 mins in the simulated process.

375 In summary, the predictive model in this study shows the potential to predict the
376 mechanical properties of 3D printed structures. The study also proves that geometric
377 features represented by entropy vectors have a strong correlation with mechanical
378 properties in LS since R^2 ranges from 0.8 to 0.96. The highest accuracy of the predictive
379 model can also reach the level reported by previous studies. Furthermore, this method
380 has the following advantages:

- 381 (1) The model can predict the mechanical properties of one LS unit in a matter of seconds.
- 382 (2) The model is suitable for different types of structures and predicts the mechanical
383 properties of LS made of different materials.
- 384 (3) The model exhibits the potential to predict other properties of LS, such as permeability
385 and failure mode.

386 **5. CONCLUSIONS**

387
388 To investigate an effective method to predict the mechanical properties of LS, this study
389 proposed a novel method based on machine learning that extracts the entropy vector
390 from LS unit 3D models to represent the geometric features of LS, in combination with
391 other commonly designed parameters as input features. The predictive model was then
392 built using SVR. The results include the following:

- 393 (1) Entropy vectors can effectively represent the geometric features of LS. Similar shapes
394 of entropy distributions are observed in the same types of structures, while the
395 distribution shape varies between different types of structures; dividing the subspaces
396 along the compression direction can eliminate the differences caused by the random
397 dividing direction.

398 (2) This study collected 57 LS samples, and the model to predict the elastic modulus of LS
399 was successfully built based on SVR. For elastic modulus, RMSE was measured at 636.48
400 and R^2 at 0.93 for the training set; for the test set, RMSE was 885.7 and R^2 was 0.81. For
401 yield strength, R^2 and mean predicted error ranged from 0.8 to 0.96 and 14.14 MPa to
402 37.14 MPa, respectively. This indicates that the chosen input features have a strong
403 correlation with the mechanical properties of LS.

404 (3) Compared with common predicted methods, the current method can reach the
405 accuracy of other methods and is not limited by materials and LS categories. In particular,
406 the predicted time is reduced from tens of minutes to a few seconds, which can greatly
407 improve the efficiency of the design process.

408 In summary, compared with the high-cost experimental method and the time-consuming
409 simulated method, this study proposes a prediction method for the elastic modulus of LS
410 that has genuine potential application value. It has the advantage of being applicable to
411 various kinds of structures and materials, while other methods based on machine learning
412 and formulae can only be applied to one kind of structure. This study is significant as it
413 can improve the efficiency of designing lattice structures, thereby reducing time and costs
414 in the design phase.

415 Future studies will consider the processing parameters of the SLM machine, the expected
416 relative density, and the manufacturing errors of structures to enhance prediction
417 accuracy. The study of predicting the failure modes of lattice structures will also be of
418 interest.

419

420 **ACKNOWLEDGMENT**

421

422 The authors would like to thank Zhihang Li and Fuyu Guo (Chongqing University) for
423 programming assistance, Xiaojie Fan (Chongqing University) for collecting data of
424 samples.

425 **FUNDING**

426 • The National Natural Science Foundation of China (Grant No: 51975073, No.
427 51805052).

428 • The China Scholarship Council (CSC).

429

430 **REFERENCES**

- 431 [1] Lei H, Li C, Meng J, Zhou H, Liu Y, Zhang X, Wang P and Fang D., 2019, "Evaluation
432 of compressive properties of SLM-fabricated multi-layer lattice structures by
433 experimental test and μ -CT-based finite element analysis," *Materials &*
434 *Design*,169:107685. 10.1016/j.matdes.2019.107685
- 435
436 [2] Jin N, Yan Z, Wang Y, Cheng H and Zhang H., 2021, "Effects of heat treatment on
437 microstructure and mechanical properties of selective laser melted Ti-6Al-4V lattice
438 materials," *International Journal of Mechanical Sciences*,190:106042.
439 10.1016/j.ijmecsci.2020.106042
- 440
441 [3] Li P, Ma Y E, Sun W, Qian X, Zhang W and Wang Z., 2021, "Fracture and failure
442 behavior of additive manufactured Ti6Al4V lattice structures under compressive load,"
443 *Engineering Fracture Mechanics*,244:107537. 10.1016/j.engfracmech.2021.107537
- 444
445 [4] Zhang L, Feih S, Daynes S, Chang S, Wang M Y, Wei J and Lu W F., 2018, "Energy
446 absorption characteristics of metallic triply periodic minimal surface sheet structures
447 under compressive loading," *Additive Manufacturing*,23:505-515.
448 10.1016/j.addma.2018.08.007
- 449
450 [5] Feng Q, Tang Q, Liu Y, Setchi R, Soe S, Ma S and Bai L., 2018, "Quasi-static analysis
451 of mechanical properties of Ti6Al4V lattice structures manufactured using selective laser
452 melting," *The International Journal of Advanced Manufacturing Technology*,94(5-8):2301-
453 2313. 10.1007/s00170-017-0932-7
- 454
455 [6] Ma S, Tang Q, Feng Q, Song J, Han X and Guo F., 2019, "Mechanical behaviours
456 and mass transport properties of bone-mimicking scaffolds consisted of gyroid structures
457 manufactured using selective laser melting," *Journal of the Mechanical Behavior of*
458 *Biomedical Materials*,93:158-169. 10.1016/j.jmbbm.2019.01.023
- 459
460 [7] Song J, Tang Q, Feng Q, Ma S, Setchi R, Liu Y, Han Q, Fan X and Zhang M., 2019,
461 "Effect of heat treatment on microstructure and mechanical behaviours of 18Ni-300
462 maraging steel manufactured by selective laser melting," *Optics & Laser*
463 *Technology*,120:105725. <https://doi.org/10.1016/j.optlastec.2019.105725>
- 464
465 [8] Zhang L, Song B, Choi S and Shi Y., 2021, "A Topology Strategy to Reduce Stress
466 Shielding of Additively Manufactured Porous Metallic Biomaterials," *International Journal*
467 *of Mechanical Sciences*:106331.
- 468
469 [9] Ma S, Tang Q, Han X, Feng Q, Song J, Setchi R and Liu Y, et al., 2020,
470 "Manufacturability, Mechanical Properties, Mass-Transport Properties and
471 Biocompatibility of Triply Periodic Minimal Surface (TPMS) Porous Scaffolds Fabricated by
472 Selective Laser Melting," *Materials & Design*,195:109034. 10.1016/j.matdes.2020.109034

473

474 [10] Alqahtani N, Armstrong R T and Mostaghimi P. Deep learning convolutional neural
475 networks to predict porous media properties: SPE Asia Pacific oil and gas conference and
476 exhibition, 2018[C]. Society of Petroleum Engineers.

477

478 [11] Wu J, Yin X and Xiao H., 2018, "Seeing permeability from images: fast prediction
479 with convolutional neural networks," *Science Bulletin*,63(18):1215-1222.
480 10.1016/j.scib.2018.08.006

481

482 [12] Ma S, Tang Q, Liu Y and Feng Q., 2021, "Predicting Mechanical Properties of 3d
483 Printed Lattice Structures," ASME Paper No. DETC2021-70249

484

485 [13] Choy S Y, Sun C, Leong K F and Wei J., 2017, "Compressive properties of Ti-6Al-4V
486 lattice structures fabricated by selective laser melting: Design, orientation and density,"
487 *Additive Manufacturing*,16:213-224. <https://doi.org/10.1016/j.addma.2017.06.012>

488

489 [14] Maskery I, Sturm L, Aremu A O, Panesar A, Williams C B, Tuck C J, Wildman R D,
490 Ashcroft I A and Hague R J M., 2018, "Insights into the mechanical properties of several
491 triply periodic minimal surface lattice structures made by polymer additive
492 manufacturing," *Polymer*,152:62-71. 10.1016/j.polymer.2017.11.049

493

494 [15] Arjunan A, Demetriou M, Baroutaji A and Wang C., 2019, "Mechanical
495 performance of highly permeable laser melted Ti6Al4V bone scaffolds," *Journal of the
496 Mechanical Behavior of Biomedical Materials*:103517.
497 <https://doi.org/10.1016/j.jmbbm.2019.103517>

498

499 [16] Hazlehurst K, Wang C J and Stanford M., 2013, "Evaluation of the stiffness
500 characteristics of square pore CoCrMo cellular structures manufactured using laser
501 melting technology for potential orthopaedic applications," *Materials & Design*,51:949-
502 955. <https://doi.org/10.1016/j.matdes.2013.05.009>

503

504 [17] Munford M, Hossain U, Ghouse S and Jeffers J R T., 2020, "Prediction of anisotropic
505 mechanical properties for lattice structures," *Additive Manufacturing*,32:101041.
506 10.1016/j.addma.2020.101041

507

508 [18] Benedetti M, Klarin J, Johansson F, Fontanari V, Luchin V, Zappini G and Molinari
509 A., 2019, "Study of the Compression Behaviour of Ti6Al4V Trabecular Structures Produced
510 by Additive Laser Manufacturing," *Materials*,12(9):1471. 10.3390/ma12091471

511

512 [19] Han C, Yan C, Wen S, Xu T, Li S, Liu J, Wei Q and Shi Y., 2017, "Effects of the unit
513 cell topology on the compression properties of porous Co-Cr scaffolds fabricated via
514 selective laser melting," *RAPID PROTOTYPING JOURNAL*,23(1):16-27. 10.1108/RPJ-08-
515 2015-0114

516

- 517 [20] Hassanin H, Alkendi Y, Elsayed M, Essa K and Zweiri Y., 2020, "Controlling the
518 Properties of Additively Manufactured Cellular Structures Using Machine Learning
519 Approaches," *Advanced Engineering Materials*,22(3):1901338.
520 10.1002/adem.201901338
521
- 522 [21] Taylor M, Perilli E and Martelli S., 2017, "Development of a surrogate model based
523 on patient weight, bone mass and geometry to predict femoral neck strains and fracture
524 loads," *Journal of Biomechanics*,55:121-127. 10.1016/j.jbiomech.2017.02.022
525
- 526 [22] Zhang M, Gong H, Zhang K and Zhang M., 2019, "Prediction of lumbar vertebral
527 strength of elderly men based on quantitative computed tomography images using
528 machine learning," *Osteoporosis International*,30(11):2271-2282. 10.1007/s00198-019-
529 05117-0
530
- 531 [23] Deng Z, Yin H, Jiang X, Zhang C, Zhang G, Xu B and Yang G, et al., 2020, "Machine-
532 learning-assisted prediction of the mechanical properties of Cu-Al alloy," *International
533 Journal of Minerals, Metallurgy and Materials*,27(3):362-373. 10.1007/s12613-019-1894-
534 6
535
- 536 [24] Furuya T and Ohbuchi R., 2018, "Learning part-in-whole relation of 3D shapes for
537 part-based 3D model retrieval," *Computer Vision and Image Understanding*,166:102-114.
538 10.1016/j.cviu.2017.11.007
539
- 540 [25] Kim H, Cha M and Mun D., 2017, "Shape distribution-based approach to
541 comparing 3D CAD assembly models," *Journal of Mechanical Science and
542 Technology*,31(12):5627-5638. 10.1007/s12206-017-1103-3
543
- 544 [26] Lu Z, Guo J, Xiao J, Wang Y, Zhang X and Yan D., 2021, "Extracting Cycle-aware
545 Feature Curve Networks from 3D Models," *Computer-Aided Design*,131:102949.
546 10.1016/j.cad.2020.102949
547
- 548 [27] Makem J E, Fogg H J and Mukherjee N., 2020, "Automatic Feature Recognition
549 Using the Medial Axis for Structured Meshing of Automotive Body Panels," *Computer-
550 Aided Design*,124:102845. 10.1016/j.cad.2020.102845
551
- 552 [28] Kim S, Chi H and Ramani K., 2021, "Object Synthesis by Learning Part Geometry
553 with Surface and Volumetric Representations," *Computer-Aided Design*,130:102932.
554 10.1016/j.cad.2020.102932
555
- 556 [29] Wei L and Yuanjun H., 2008, "Representation and retrieval of 3D CAD models in
557 parts library," *The International Journal of Advanced Manufacturing Technology*,36(9-
558 10):950-958. 10.1007/s00170-006-0914-7
559

- 560 [30] Maskery I, Aboulkhair N T, Aremu A O, Tuck C J and Ashcroft I A., 2017,
561 "Compressive failure modes and energy absorption in additively manufactured double
562 gyroid lattices," *Additive Manufacturing*,16:24-29. 10.1016/j.addma.2017.04.003
563
- 564 [31] Bartolomeu F, Costa M M, Alves N, Miranda G and Silva F S., 2021, "Selective Laser
565 Melting of Ti6Al4V sub-millimetric cellular structures: Prediction of dimensional
566 deviations and mechanical performance," *Journal of the Mechanical Behavior of*
567 *Biomedical Materials*,113:104123. 10.1016/j.jmbbm.2020.104123
568
- 569 [32] Atae A, Li Y, Brandt M and Wen C., 2018, "Ultrahigh-strength titanium gyroid
570 scaffolds manufactured by selective laser melting (SLM) for bone implant applications,"
571 *ACTA MATERIALIA*,158:354-368. 10.1016/j.actamat.2018.08.005
572
- 573 [33] Wang S, Liu L, Zhou X, Zhu L and Hao Y., 2020, "The design of Ti6Al4V Primitive
574 surface structure with symmetrical gradient of pore size in biomimetic bone scaffold,"
575 *Materials & Design*,193:108830.
576
- 577 [34] Liao B, Xia R F, Li W, Lu D and Jin Z M., 2021, "3D-Printed Ti6Al4V Scaffolds with
578 Graded Triply Periodic Minimal Surface Structure for Bone Tissue Engineering," *Journal of*
579 *Materials Engineering and Performance*, 10.1007/s11665-021-05580-z
580
581

582
583

Figure Captions List

- FIGURE 1 (a) BCC structure unit; (b) BCCZ structure unit; (c) TPMS structure units.
- FIGURE 2 Ti6AL4V bone scaffold composed of gyroid structures
- FIGURE 3 Schematic diagram of voxelisation
- FIGURE 4 Process of dividing subspace and calculating entropy vector
- FIGURE 5 Featured parameters of (a) strut structures; (b) TPMS structures; (c) common parameters of all lattice structures.
- FIGURE 6 Process of predicting mechanical properties of LS units by machine learning
- FIGURE 7 Elastic modulus of training set: (a) actual/predicted values; (b) relative error.
- FIGURE 8 Elastic modulus of test set: (a) actual/predicted values; (b) relative error.
- FIGURE 9 Yield strength of training set: (a) actual/predicted values; (b) relative error.
- FIGURE 10 Yield strength of test set: (a) actual/predicted values; (b) relative error.

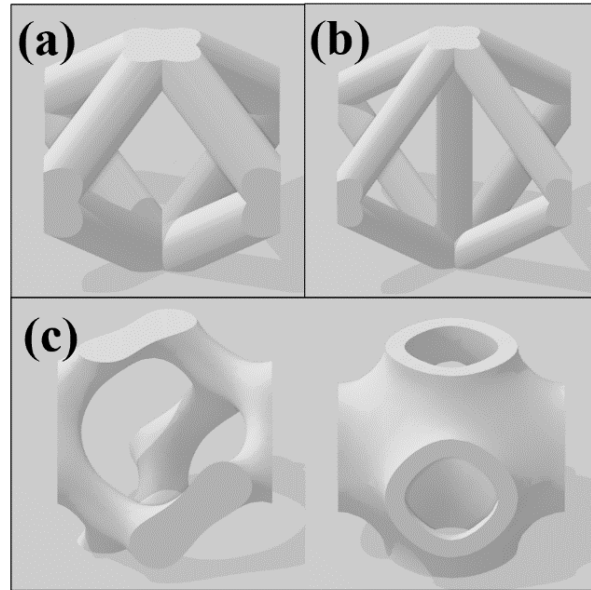
584
585

586
587

Table Caption List

Table 1	Categories of studied LS samples
Table 2	Results of entropy distributions of different LS units
Table 3	Evaluation of the predictive model in training set and test set
Table 4	Comparison of errors in previous and current studies
Table 5	Comparison of formula, FEA, and current methods

588
589



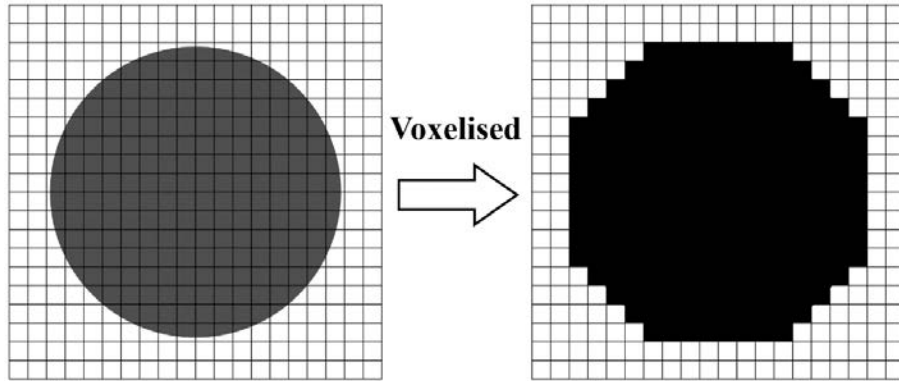
590
591
592

FIGURE 1: (a) BCC structure unit; (b) BCCZ structure unit; (c) TPMS structure units.



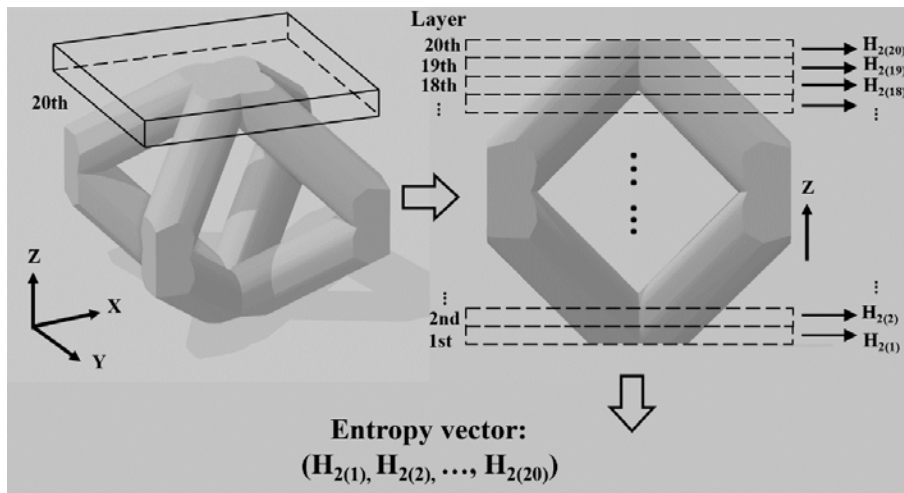
593
594
595
596

FIGURE 2: Ti6AL4V bone scaffold composed of gyroid structures



597
598
599
600

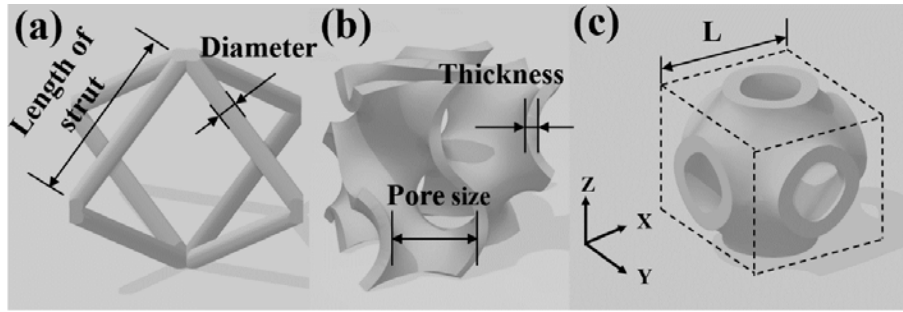
FIGURE 3: Schematic diagram of voxelisation



601
602
603

FIGURE 4: Process of dividing subspace and calculating entropy vector

604



605

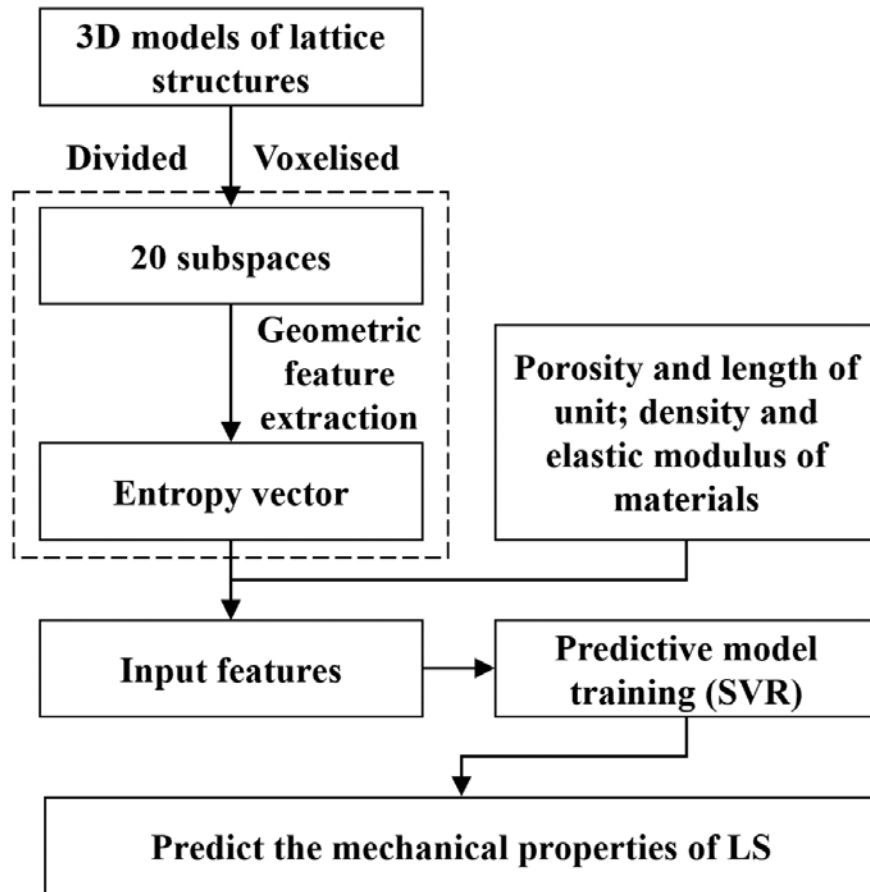
606

607

608

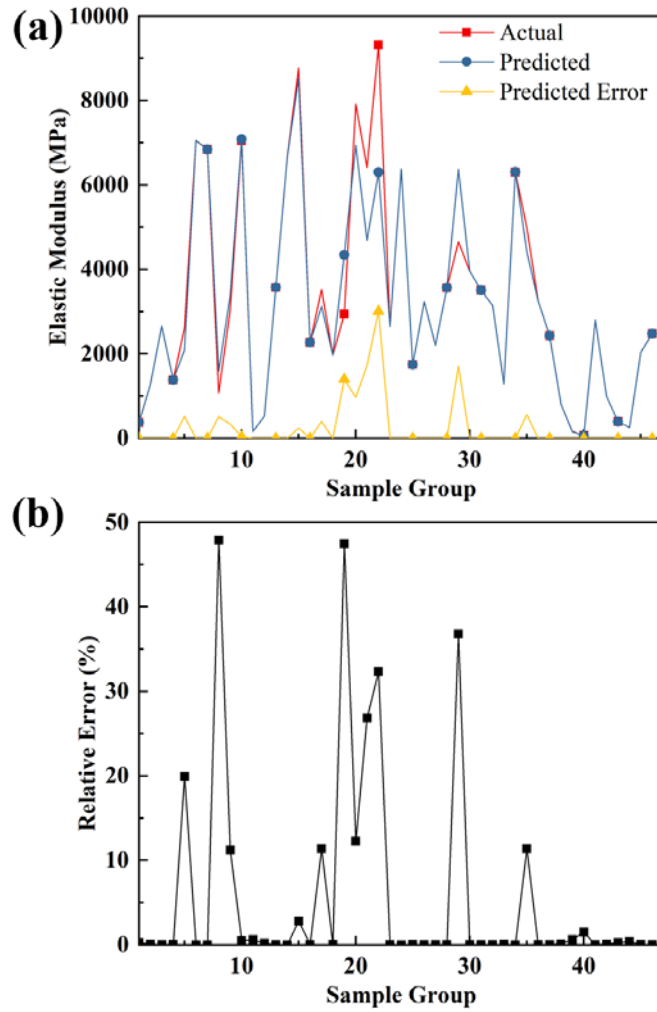
FIGURE 5: Featured parameters of (a) strut structures, (b) TPMS structures, (c) common parameters of all lattice structures.

609



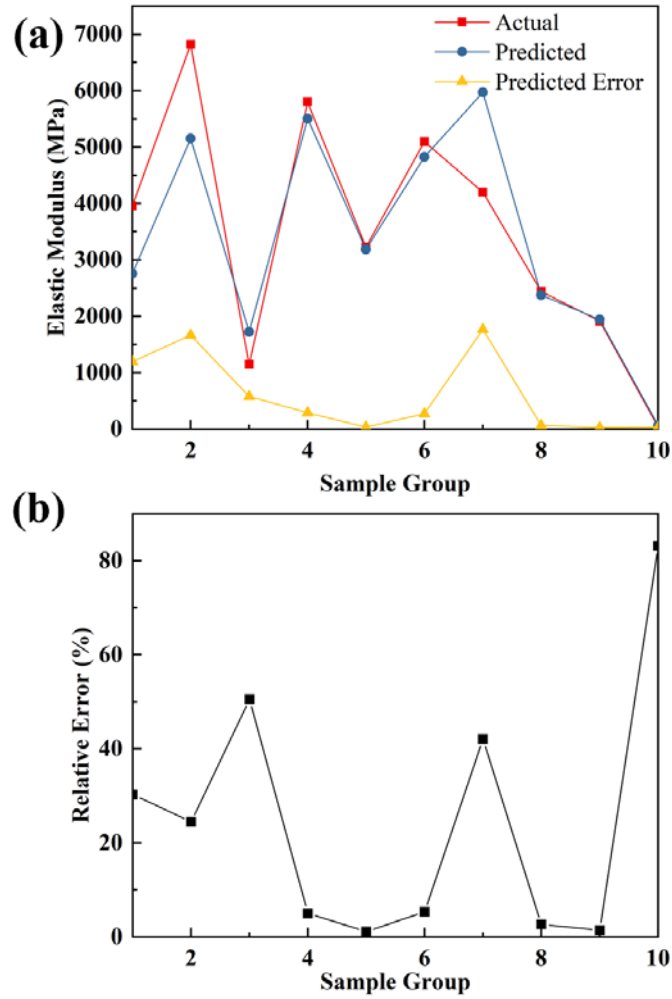
610
611
612

FIGURE 6: Process of predicting mechanical properties of LS units by machine learning



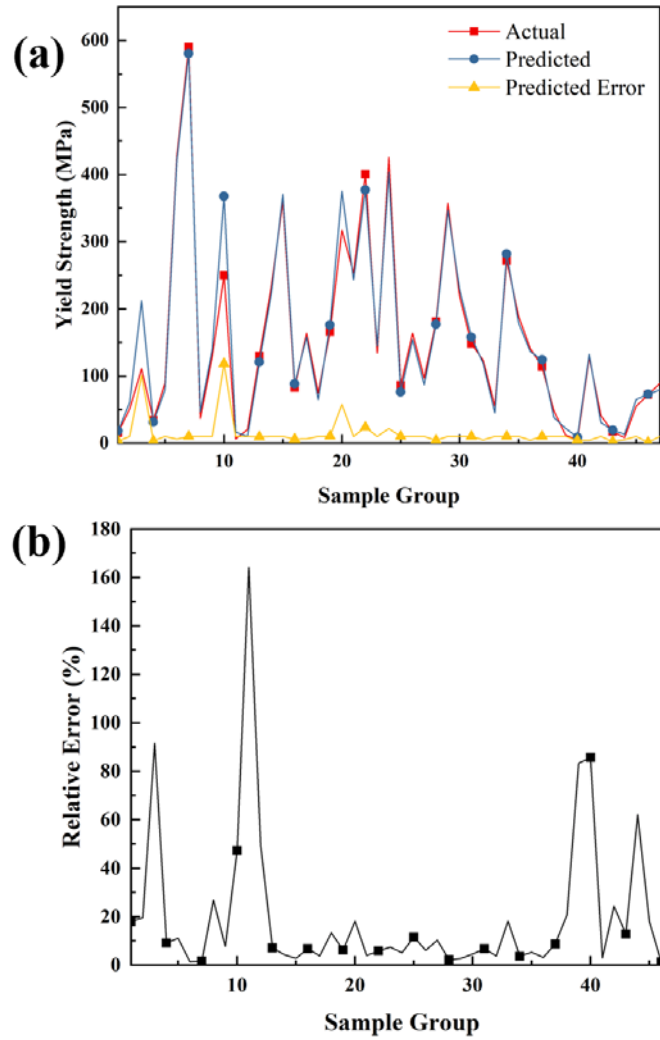
613
614
615

FIGURE 7: Elastic modulus of training set: (a) actual/predicted values; (b) relative error.



616
617
618

FIGURE 8: Elastic modulus of test set: (a) actual/predicted values; (b) relative error.



619
620
621

FIGURE 9: Yield strength of training set: (a) actual/predicted values; (b) relative error.

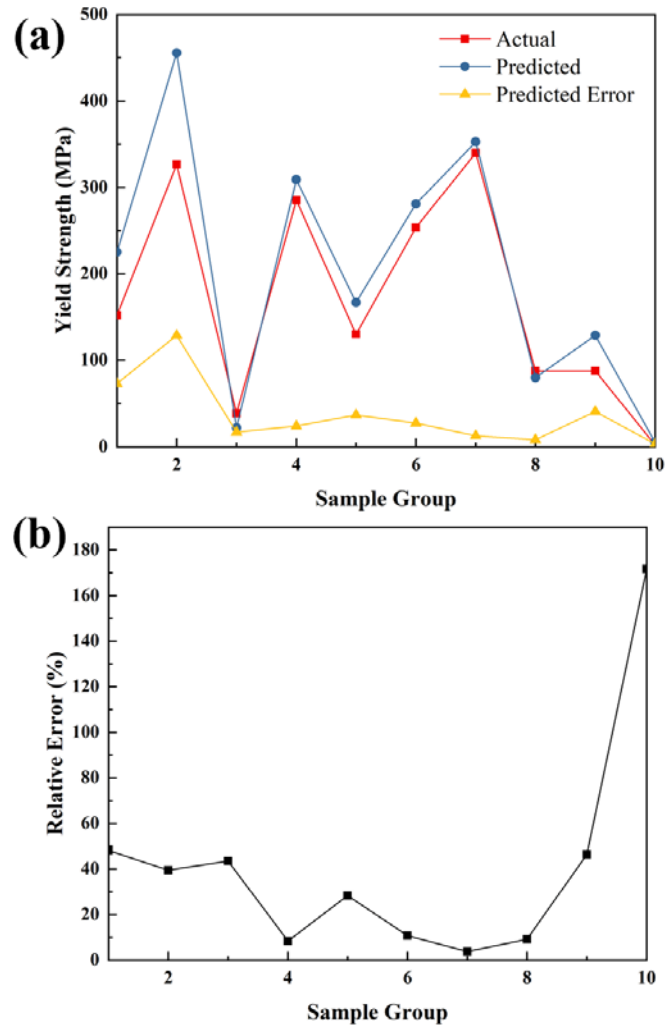


FIGURE 10: Yield strength of test set: (a) actual/predicted values; (b) relative error.

622
623
624

TABLE 1: Categories of studied LS samples


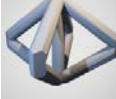









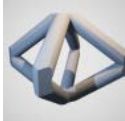

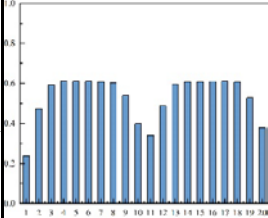
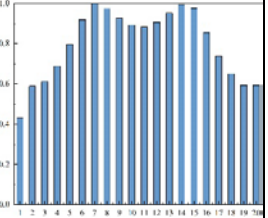

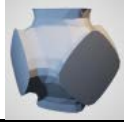
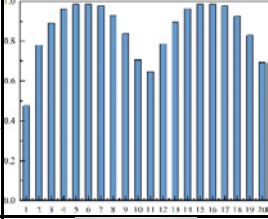
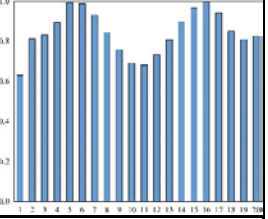


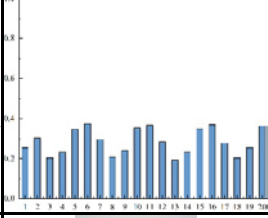
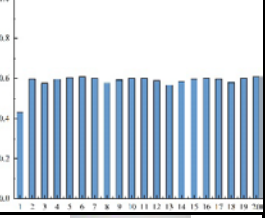


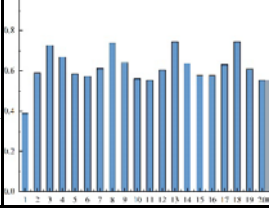
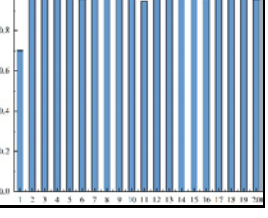
Category number	3D model	Structure type	Number of samples
1		BCC	7
2		BCCZ	3
3		Strut-based Schwarz primitive	8
4		Strut-based diamond	3
5		Strut-based gyroid	3
6		Strut-based diamond	3
7		Sheet-based gyroid	9
8		Sheet-based Schwarz primitive	11
9		Sheet-based I-WP	3
10		Neovius	3
11		FCC	4

TABLE 2: Results of entropy distributions of different LS units

LS unit		
Entropy distribution		
LS unit		
Entropy distribution		
LS unit		
Entropy distribution		
LS unit		
Entropy distribution		

630

TABLE 3: Evaluation of the predictive model in training set and test set

	Set	RMSE	R ²	Mean error (MPa)	Mean e _r (%)
Elastic modulus	Training set	636.48	0.93	244.11	5.66
	Test set	885.70	0.81	593.72	24.61
Yield strength	Training set	25.96	0.96	14.14	20.1
	Test set	51.74	0.80	37.14	40.9

631

632

633

634

TABLE 4: Comparison of errors in previous and current studies

	Elastic modulus range (MPa)	Error (MPa)	Yield strength range (MPa)	Error (MPa)
[32]	1465 ~ 2676	33 ~ 162	-	
[33]	2700 ~ 3600	100 ~ 130	-	
[16]	1060 ~ 28590	120 ~ 3640	9.3 ~ 327.47	0.38 ~ 12
[34]	2700 ~ 7400	100 ~ 400	233 ~ 520	3 ~ 60
Current study	37.5 ~ 9309	244 ~ 593	1.9 ~ 590.3	14.14 ~ 37.14

635

636

637

638

TABLE 5: Comparison of formula, FEA, and current methods

	Error of elastic modulus (MPa)			Error of yield strength (MPa)		
	Formula	FEA	SVR	Formula	FEA	SVR
BCC 1	117	521	1	-	8	10
BCC 2	23	60	1	-	2.5	10
BCC 3	24.5	67.5	1	-	1.15	4.03
BCC 4	19.5	10.5	31	-	0.375	3.26
Fcc-BCC 1	-	2200	1	-	14	3.81
Fcc-BCC 2	-	407	1	-	13.5	10
Fcc-BCC 3	-	170	1	-	4.5	2.2
Fcc-BCC 4	-	56	1	-	1.1	5.03
Average time	-	~ 30 mins	~ 5 secs	-	~ 30 mins	~ 5 secs

639

640